



Cite this: *Phys. Chem. Chem. Phys.*,  
2018, 20, 15841

## Membrane potential and dynamics in a ternary lipid mixture: insights from molecular dynamics simulations†

Xubo Lin, <sup>ab</sup> Vinay Nair, <sup>a</sup> Yong Zhou <sup>a</sup> and Alemayehu A. Gorfe <sup>a\*</sup>

Transmembrane potential ( $V_m$ ) plays critical roles in cell signaling and other functions. However, the impact of  $V_m$  on the structure and dynamics of membrane lipids and proteins, which are critical for the regulation of signaling, is still an open question. All-atom molecular dynamics (MD) simulation is emerging as a useful technique to address this issue. Previous atomistic MD simulations of pure or binary model membranes indicated that both ion imbalance and electric field can be used to generate  $V_m$ , but both approaches failed to yield structural changes in lipids with statistical significance. We hypothesized that a possible reason for this could be oversimplified membrane composition or limited sampling. In this work, we tested if and how  $V_m$  modulates the structure and dynamics of lipids in a physiologically relevant model membrane. Using a detailed side-by-side comparison, we first show that while both ion imbalance and electric field generate  $V_m$  in our complex membranes, only the latter could produce physiologically relevant  $V_m$ . We further show that double bonds in lipid acyl chains have a relatively large sensitivity to  $V_m$ . A single-bilayer model with an electric field showed the highest sensitivity in simulations under the isothermal-isobaric (NPT) ensemble, reproducing expected responses of head-group dipoles to  $V_m$  and suggesting that this approach may be more suitable for studying the structural effects of  $V_m$ . Our findings also shed light on the relationship between the macroscopic  $V_m$  and its atomic-level underpinnings.

Received 13th March 2018,  
Accepted 15th May 2018

DOI: 10.1039/c8cp01629a

rsc.li/pccp

## Introduction

The plasma membrane (PM) is a selectively permeable barrier between the intra- and extra-cellular environments of eukaryotic cells. The differential distribution of ions across the PM generates a transmembrane potential ( $V_m$ ) of approximately  $-40$  to  $-90$  mV in non-proliferating cells.<sup>1</sup> Proliferating cancer cells, on the other hand, tend to have a smaller  $V_m$  (*i.e.*, are depolarized), which is believed to contribute to their increased migration and differentiation.<sup>1–3</sup> Recently, Zhou *et al.* showed that PM depolarization enhances K-Ras clustering and increases mitogen-activated protein kinase (MAPK) signaling, thus promoting cell proliferation.<sup>4</sup> It was proposed that  $V_m$ -induced change in K-Ras clustering is coupled with the reorganization of anionic lipids, especially phosphatidylserine (PS) and phosphatidylinositol 4,5-bisphosphate (PI(4,5)P<sub>2</sub> or PIP2). Similarly, Chatterjee *et al.* found that PM depolarization triggers the activation of the

PI3K/AKT signaling pathway and induces the generation of reactive oxygen species (ROS), which may contribute to carcinogenesis.<sup>5</sup> The authors speculated that the voltage-sensitive domain of PI3K or phosphatase-mediated changes in substrate concentration might be responsible for the  $V_m$ -induced activation of PI3K. However, in both cases, the mechanisms by which  $V_m$  induces changes in the structure and/or dynamics of PM lipids remain unexplored.

There are various approaches to measure  $V_m$  experimentally, including patch clamping<sup>6,7</sup> and *in situ* optical measurements with voltage-sensitive fluorescent probes.<sup>8,9</sup> Computational approaches can complement these experiments by connecting macroscopic observations with the atomic origin of  $V_m$ . Atomistic molecular dynamics (MD) simulation is particularly suited for studying electrophysiology *in silico*.<sup>10–14</sup> MD simulation allows for studying the potential impact of  $V_m$  on the structure and dynamics of individual lipids and their re-organization.<sup>15</sup> When used in conjunction with a large pulsed electric field, MD can also reproduce membrane electroporation observed by low-volt, long-duration pulses in experiments.<sup>16,17</sup> However, previous MD studies of  $V_m$  focused mostly on pure bilayers such as the bilayers of 1-palmitoyl-2-oleoyl-sn-glycero-3-phosphocholine (POPC),<sup>10,14</sup> 1,2-dipalmitoyl-sn-glycero-3-phosphocholine (DPPC)<sup>12,17</sup> and 1,2-dimyristoyl-sn-glycero-3-phosphocholine (DMPC)<sup>18</sup> lipids. It has

<sup>a</sup> Department of Integrative Biology and Pharmacology, McGovern Medical School, The University of Texas Health Science Center at Houston, Texas 77030, USA

<sup>b</sup> Beijing Advanced Innovation Center for Biomedical Engineering, School of Biological Science and Medical Engineering, Beihang University, Beijing 100083, China. E-mail: alemayehu.g.abebe@uth.tmc.edu

† Electronic supplementary information (ESI) available: The convergence of  $V_m$  calculations, additional order parameters and system snapshots. See DOI: 10.1039/c8cp01629a

been shown that application of ion imbalance or external electric field to a model membrane can generate  $V_m$  during simulations. In both approaches, however, even  $V_m$  values as large as  $\sim 450$  mV did not appear to result in significant structural changes in the bilayer.<sup>14</sup> Thus, whether  $V_m$  can indeed induce measurable structural changes in membrane lipids during MD is still unclear. Experiments have shown that lipid head-groups and water dipoles align along electric fields<sup>19</sup> and thereby induce membrane structural changes and even poration. Failure to observe the structural effects of  $V_m$  in MD simulations may therefore be a consequence of limited sampling of the configurational space or the use of small voltage amplitudes and oversimplified model membranes. In the current work, we added the anionic lipid 1-palmitoyl-2-oleoyl-sn-glycero-3-phospho-l-serine (POPS) and the highly charged PIP2 to the previously simulated neutral POPC lipid bilayers. This mixture more faithfully models the PM of mammalian cells and was used in our all-atom MD simulations in the presence of a wide range of  $V_m$  generated by applied electric fields or externally imposed imbalance of ion distributions. Our goal was to examine subtle changes in the structure and dynamics of both lipid head-groups and acyl chains as a function of changes in  $V_m$ . We found that lipid head-groups and double bonds at the acyl chains are particularly sensitive to changes in  $V_m$ .

## Methods

### System construction

$V_m$  can be generated during MD through an inter-monolayer imbalance of ions ( $Q$ )<sup>10,12–14</sup> or via the application of an external electric field ( $E$ ).<sup>10,14,20,21</sup> The former can be modeled in a single-bilayer by adding a vacuum at each side of the bilayer,<sup>10</sup> or in a double-bilayer in which the inter-bilayer compartment has a different ion content than the outer chambers.<sup>12</sup> Using a double bilayer lets us study two bilayers in a single simulation, resulting in better sampling. The goal in each case is to prevent the spontaneous redistribution and equalization of the number of ions. The electric field, on the hand, can be applied directly to a single-bilayer system with or without a vacuum.<sup>20,21</sup> We tested all these approaches in the current work (Table 1 and Fig. 1a).

To model the PM of mammalian cells as closely as possible,<sup>22,23</sup> we built a ternary bilayer made up of 280 POPC (70%), 100 POPS (25%) and 20 PIP2 (5%) using the CHARMM-GUI membrane builder<sup>24,25</sup> and added 28732 TIP3P water molecules plus 200  $\text{Na}^+$  counter ions to achieve overall charge

neutrality. Based on this, we set up 18 simulation systems (plus 3 control simulations without PIP2) with either ion imbalance or an electric field used to generate  $V_m$  (Table 1). To model ion imbalance ( $\Delta Q$ ) while maintaining overall charge neutrality, we moved 1–5  $\text{Na}^+$  ions from one monolayer to the other, yielding  $\Delta Q = 2, 4, 6, 8$  or 10 in the single-bilayer systems and  $\Delta Q = 1$  or 2 in the double-bilayer systems. To model an electric field,  $f_{i,q} = q_i E_z$  was added to the classical (unmodified) force  $f_{i0}$  on each atom  $i$  with partial charge  $q_i$ , where  $E_z$  is the external electric field directed along the  $z$ -axis (in this case, Newton's equation of motion becomes  $m_i \ddot{r}_i = f_{i0} + f_{i,q}$ ).  $E_z$  is continuously adjustable. Here, we choose 8.8 mV nm<sup>−1</sup> as the non-zero minimum value that may be able to generate physiologically relevant  $V_m$ . GROMACS 5.0.4 supports the application of both constant and time-varied electric fields;<sup>26</sup> we used the constant electric field in the current work.

### Molecular dynamics simulation

All simulations were conducted with GROMACS<sup>26</sup> using the CHARMM36 force field for lipids<sup>27</sup> and the standard CHARMM parameters for ions<sup>28</sup> and water.<sup>29</sup> The Lennard-Jones potential was smoothly shifted to zero between 1.0 and 1.2 nm. Particle-Mesh Ewald (PME) electrostatics<sup>30</sup> was used with a real-space cutoff of 1.2 nm. Lipids and solvent were coupled separately to a Nosé-Hoover heat bath<sup>31,32</sup> at  $T = 310$  K (coupling constant  $\tau = 1$  ps); a pressure of 1 bar was maintained by a semi-isotropic Parrinello-Rahman pressure coupling scheme<sup>33</sup> with a coupling constant  $\tau = 5$  ps and a compressibility of  $4.5 \times 10^{-5}$  bar<sup>−1</sup>. Simulations were conducted with a 2 fs time-step, restraining all bonds involving hydrogen atoms with the LINCS algorithm.<sup>34</sup> Non-bonded neighbor lists were updated every 20 steps with a cutoff of 1.2 nm. Each simulation was run for 0.3 or 1  $\mu\text{s}$ , saving the coordinates every 2 ps for analysis. Snapshots were rendered by VMD.<sup>35</sup>

### Electrostatic potential across membrane

Electrostatic potential across membrane,  $\psi(z)$ , is calculated using the Poisson equation<sup>10</sup> involving the double integral of the charge density  $\rho(z)$  along the membrane normal ( $z$ ):

$$\psi(z) = -\frac{1}{\varepsilon_0} \int_{-z}^z dz' \int_{-z'}^{z'} \rho(z'') dz'' \quad (1)$$

To minimize the error from fluctuations of the simulation box in the db and sb systems, we set the center-of-mass of the bilayer to the origin and calculated the charge densities  $\rho(z)$

Table 1 Summary of the simulations performed in this work

System <sup>a</sup>	$Q_0^{\text{sbv}}$	$Q_2^{\text{sbv}}$	$Q_4^{\text{sbv}}$	$Q_6^{\text{sbv}}$	$Q_8^{\text{sbv}}$	$Q_{10}^{\text{sbv}}$	$E_0^{\text{sbv}}$	$E_{8.8}^{\text{sbv}}$	$E_{17.6}^{\text{sbv}}$	$E_{26.4}^{\text{sbv}}$	$E_{88}^{\text{sbv}}$	$E_{176}^{\text{sbv}}$	$Q_0^{\text{db}}$	$Q_1^{\text{db}}$	$Q_2^{\text{db}}$	$E_0^{\text{sb}}$	$E_{88}^{\text{sb}}$	$E_{176}^{\text{sb}}$
$\Delta Q (e)$	0	2	4	6	8	10	—	—	—	—	—	—	0	1	2	—	—	—
$E_z (\text{mV nm}^{-1})$	—	—	—	—	—	—	0	8.8	17.6	26.4	88	176	—	—	—	0	88	176
Length ( $\mu\text{s}$ )	0.3	0.3	0.3	0.3	0.3	0.3	0.3	0.3	0.3	0.3	0.3	0.3	1	1	1	0.3	0.3	0.3
$V_m$ (V)	0.00	0.55	1.14	1.68	2.26	2.79	0.02	0.08	0.14	0.21	0.74	1.51	0.07	0.24	0.41	0.07	0.98	1.84

<sup>a</sup> Each system is named as  $Q_x^{\text{model}}$  or  $E_x^{\text{model}}$  where  $Q$  represents ion imbalance and  $E$  represents the constant electric field; the model equals sbv (single-bilayer with vacuum), db (double-bilayer), or sb (single-bilayer);  $x$  is the value of  $Q$  per bilayer in  $e$  or the strength of  $E$  ( $E_z$ ) in mV nm<sup>−1</sup>. All the single-bilayer systems consist of 280 POPC, 100 POPS, 20 PIP2, and 28732 TIP3P water plus 200  $\text{Na}^+$ , and were simulated for 300 ns each. The double-bilayer systems are twice as large and therefore the simulations were extended to 1  $\mu\text{s}$  for better sampling. In order to examine the role of PIP2, three 1  $\mu\text{s}$ -long control simulations of the double-bilayer systems were run without PIP2, referred to as  $Q_0^{\text{db}^*}$ ,  $Q_1^{\text{db}^*}$  and  $Q_2^{\text{db}^*}$  (not listed in the table).

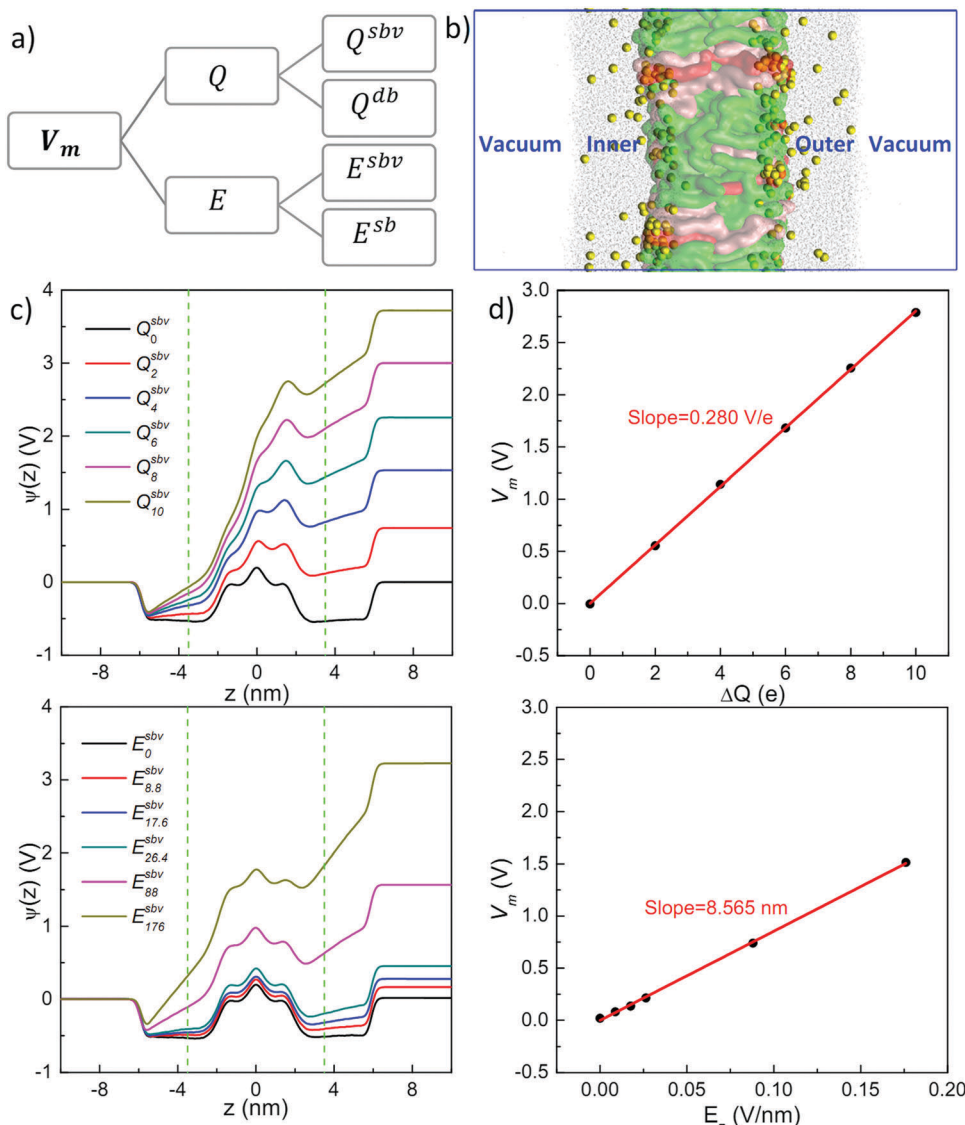


**Fig. 1**  $V_m$  modeling using  $Q_{sbv}$  and  $E_{sbv}$  approaches. (a) The approaches used in the current work for modeling  $V_m$  (see Table 1 for abbreviations). (b) A system snapshot at  $t = 0$  ns with POPC in green, POPS in pink, PIP2 in red, Na<sup>+</sup> in yellow and water in grey. (c) Electrostatic potential profile  $\psi(z)$  along the  $z$ -axis for 12 simulation systems using charge imbalance (top) and electric field (bottom). (d) A linear relationship between  $V_m$  measured as the potential difference at  $z = -3.5$  nm and  $z = +3.5$  nm (highlighted in green dashed lines in panel c) and the source of the  $V_m$ :  $Q$  (top) or  $E_z$  (bottom).  $|z| \leq 3.5$  nm encompasses the entire membrane as well as the bilayer–water interface as shown by the mass density profiles in Fig. S3a (ESI†). In panels (c and d), the analysis involved the data from the last 250 ns of each 300 ns trajectory.

and  $\psi(z)$  from  $z = -4$  to  $z = 4$  nm, which is wide enough to include bulk solvent while avoiding fluctuations at the edges of the box. As for the sbv systems, the box dimensions are fixed and therefore  $\rho(z)$  and  $\psi(z)$  were calculated along the entire  $z$  dimension from  $z = -10$  to  $z = 10$  nm after re-centering the membrane in the box for every frame of the trajectory.

#### Lipid acyl chain order parameter

The lipid chain order parameter,  $S_{CH}$ , which is a sensitive measure of the structural flexibility of lipids in a bilayer, was calculated as:

$$S_{CH} = \frac{1}{2} \langle 3 \cos^2 \theta - 1 \rangle \quad (2)$$

where  $\theta$  is the angle between the acyl chain C–H bond and the membrane normal. By calculating in this manner,  $S_{CH}$  can be directly compared to the deuterium order parameter  $S_{CD}$  measured by experiments.<sup>36,37</sup>

#### Lipid head-group orientation autocorrelation function

We define the lipid head-group orientation,  $\theta$ , as the angle between the membrane normal and a vector from atom P to atom N of a lipid, so that the head-group dipole rotation autocorrelation function,  $C(\tau)$ , can be calculated as:<sup>38</sup>

$$C(\tau) = \left\langle \frac{\sum [\theta(t) - \overline{\theta(t)}] \cdot [\theta(t + \tau) - \overline{\theta(t)}]}{\sum [\theta(t) - \overline{\theta(t)}]^2} \right\rangle \quad (3)$$

where  $\theta(t)$  and  $\theta(t + \tau)$  represent the instantaneous angles at time  $t$  and  $t + \tau$ ,  $\overline{\theta(t)}$  is the time-averaged angle and  $\langle \rangle$  denotes averaging over all selected lipids.

## Results

### Application of charge imbalance ( $Q$ ) and external electric field ( $E$ ) to generate $V_m$ in charged membranes

Charge imbalance across membranes generates an electric field and thus an electrical potential difference. Therefore, the constant  $E$  can be used to mimic the effects of ion imbalance. In fact, both  $Q$  and  $E$  are frequently used to model the transmembrane potential across bilayers. Our model membrane is a highly charged ternary mixture of POPC, POPS and PIP2 lipids that has not been studied by MD as extensively as simpler bilayer models made up of one or two lipid types.<sup>10–12,14,39,40</sup> Previous studies have shown that  $Q$  and  $E$  generate similar  $V_m$  values in a POPC bilayer.<sup>10,12</sup> However, it is not clear whether this is still valid for highly charged membranes.

As mentioned in the Methods section, both  $Q$  and  $E$  approaches can be applied to a single-bilayer model in the presence of a vacuum (systems  $Q^{\text{sbv}}$  and  $E^{\text{sbv}}$ , Fig. 1a).<sup>10</sup> In this approach, the only difference between systems  $Q^{\text{sbv}}$  and  $E^{\text{sbv}}$  is the way in which

$V_m$  is generated, which allows us to directly compare the  $Q$  and  $E$  approaches for modeling  $V_m$  of complex membranes. Therefore, we first evaluated the performance of  $Q$  and  $E$  in generating  $V_m$  in our ternary lipid bilayer using sbv modeling. To simulate a POPC/POPS/PIP2 bilayer with a vacuum, we first built a symmetric bilayer of 280 POPC (70%), 100 POPS (25%) and 20 PIP2 (5%), as described in the Methods section. After a 100 ns equilibrium run of this system under the isothermal-isobaric (*NPT*) ensemble, we placed it at the center of a new simulation box with a larger  $z$  dimension (20 nm), with the regions  $z < -6$  nm and  $z > 6$  nm representing the vacuum (Fig. 1b). To generate an ion imbalance while keeping the whole system neutral, 1–5  $\text{Na}^+$  ions were moved from the inner to the outer chamber ( $z > 0$ , Fig. 1b), and the number of water molecules was kept the same for both chambers to yield six systems:  $Q_0^{\text{sbv}}$ ,  $Q_2^{\text{sbv}}$ ,  $Q_4^{\text{sbv}}$ ,  $Q_6^{\text{sbv}}$ ,  $Q_8^{\text{sbv}}$ , and  $Q_{10}^{\text{sbv}}$  where  $Q = 0, 2, 4, 6, 8$ , and  $10\text{ e}$  (Table 1). Using the same initial bilayer model with a vacuum, we prepared systems with different  $E$  values by applying a constant electric field  $E_z$  of different strengths, resulting in systems  $E_0^{\text{sbv}}$ ,  $E_{8.8}^{\text{sbv}}$ ,  $E_{17.6}^{\text{sbv}}$ ,  $E_{26.4}^{\text{sbv}}$ ,  $E_{88}^{\text{sbv}}$ , and  $E_{176}^{\text{sbv}}$  with  $E_z = 0, 8.8, 17.6, 26.4, 88$ , and  $176\text{ mV nm}^{-1}$  (Table 1). We simulated each of these systems under the isothermal-isochoric (*NVT*) ensemble for 300 ns and compared the  $V_m$ s derived from the electrostatic potential  $\psi(z)$  based on charge density profiles (eqn (1)).

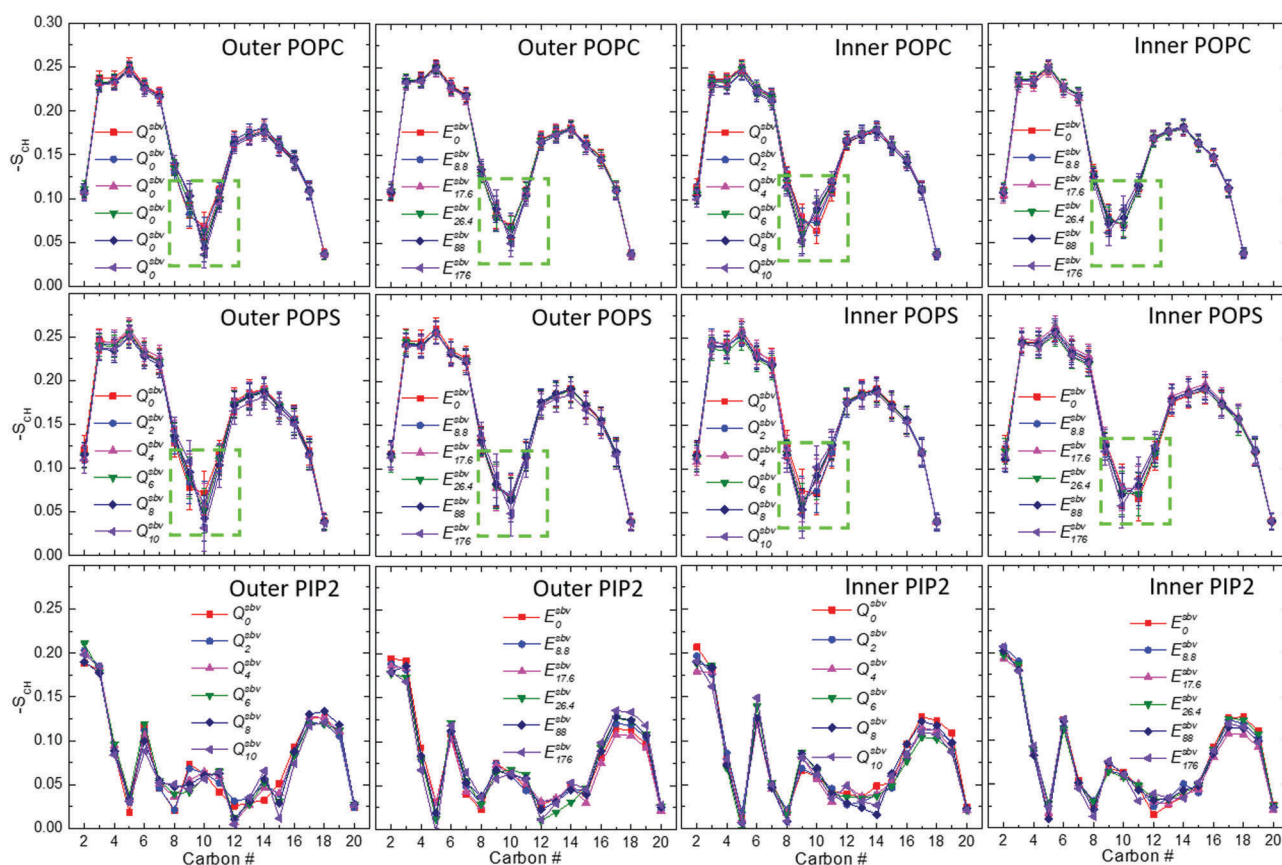


Fig. 2  $V_m$  slightly affects the lipid chain order. In both systems  $Q^{\text{sbv}}$  and  $E^{\text{sbv}}$ ,  $V_m$  has a small but significant effect on the order of the sn-2 chain, especially at the double bond (green dashed box). Though small, this effect is dependent upon  $V_m$  and the inner and outer leaflets appear to respond oppositely. The data are shown as mean  $\pm$  SEM. The statistics is poor for the minor lipid PIP2, whose error (SEM) is not shown here.

To estimate convergence, we calculated  $\psi(z)$  over different ranges of time. Fig. S1 and S2 (ESI†) show that 300 ns is adequate to obtain the converged  $\psi(z)$ . A similar observation was made for a pure POPC bilayer.<sup>14</sup> We then compared the  $\psi(z)$  obtained from systems  $Q^{\text{sbv}}$  and  $E^{\text{sbv}}$ . Fig. 1c shows that the  $\psi(z)$  profiles are qualitatively similar, supporting previous conclusions regarding the role of  $Q$  and  $E$  in modeling  $V_m$ . We defined the difference in the electrostatic potential at  $z = -3.5$  nm and  $z = +3.5$  nm as  $V_m$ , since  $|z| < 3.5$  nm encompasses the whole membrane as well as the bilayer–water interface (Fig. S3a, ESI†). We found that, irrespective of the way it was generated,  $V_m$  is linearly correlated to its source (*i.e.*,  $Q$  or  $E_z$ ; Fig. 1d). In fact, in both cases, we observed an excellent fitting of the data to a linear model. This shows that either approach can be used to model  $V_m$  in charged membranes although, as we discuss in subsequent sections, the electric field approach appears to be more suitable for generating physiologically relevant  $V_m$  values.

The  $\psi(z)$  profiles from simulations  $Q^{\text{sbv}}$  and  $E^{\text{sbv}}$  progressively diverge as  $V_m$  increases (Fig. 1c). For example, comparison of  $Q_8^{\text{sbv}}$  with  $E_{176}^{\text{sbv}}$  outside the membrane shows that  $\psi(z)$  increases more rapidly in the latter. This is because the electric field induces the ordering of water molecules at the water–vacuum interface (data not shown). In the core of the bilayer, including the bilayer mid-plane ( $z = 0$ ), the dependence of  $\psi(z)$  on the source of the potential differs. While the shape of the  $\psi(z)$  plot within the hydrophobic core remains unaffected by the strength of the electric field, it varies with  $\Delta Q$ . This is primarily because

an increasing number of  $\text{Na}^+$  gets clustered in the head-group and glycerol regions of the bilayer as  $\Delta Q$  increases (Fig. S7, ESI†). This alters the local ion distribution and thereby the electrostatic potential.

#### Potential effects of $V_m$ on the structure of membrane lipids in systems $Q^{\text{sbv}}$ and $E^{\text{sbv}}$

As shown in Fig. S3a (ESI†),  $V_m$  does not induce a major effect on the mass density profiles but, in the  $Q^{\text{sbv}}$  systems, there are small changes in the bilayer center and head-group regions that become noticeable when  $V_m$  is large (systems  $Q_8^{\text{sbv}}$  and  $Q_{10}^{\text{sbv}}$  in Fig. S3a, ESI†). This suggests that  $V_m$  may have strength-dependent structural effects on membrane lipids. Hence, we investigated the behavior of both lipid head-groups and acyl chains under different  $V_m$  values. Similar to POPC bilayers,<sup>10,14</sup> we did not observe the  $V_m$ -induced effect on the lipid head-group dynamics even with a  $V_m$  of  $\sim 2.8$  V (system  $Q_{10}^{\text{sbv}}$ ). This may be an artifact of the *NVT* ensemble used for these systems, because the fixed volume limits the collective changes in the head-group orientation that would induce a change in the lateral area. This also explains the absence of membrane poration by the large  $V_m$  in system  $Q_{10}^{\text{sbv}}$ .

Interestingly, lipid acyl chain order parameter ( $-S_{\text{CH}}$ ) analysis suggested that the double bond between carbons 9 and 10 in the sn-2 chain of POPC and POPS is somewhat sensitive to  $V_m$  (Fig. 2). Increasing  $V_m$  led to an increase of  $-S_{\text{CH}}$  at carbon 9 and a decrease of  $-S_{\text{CH}}$  at carbon 10 in the outer leaflet; the opposite

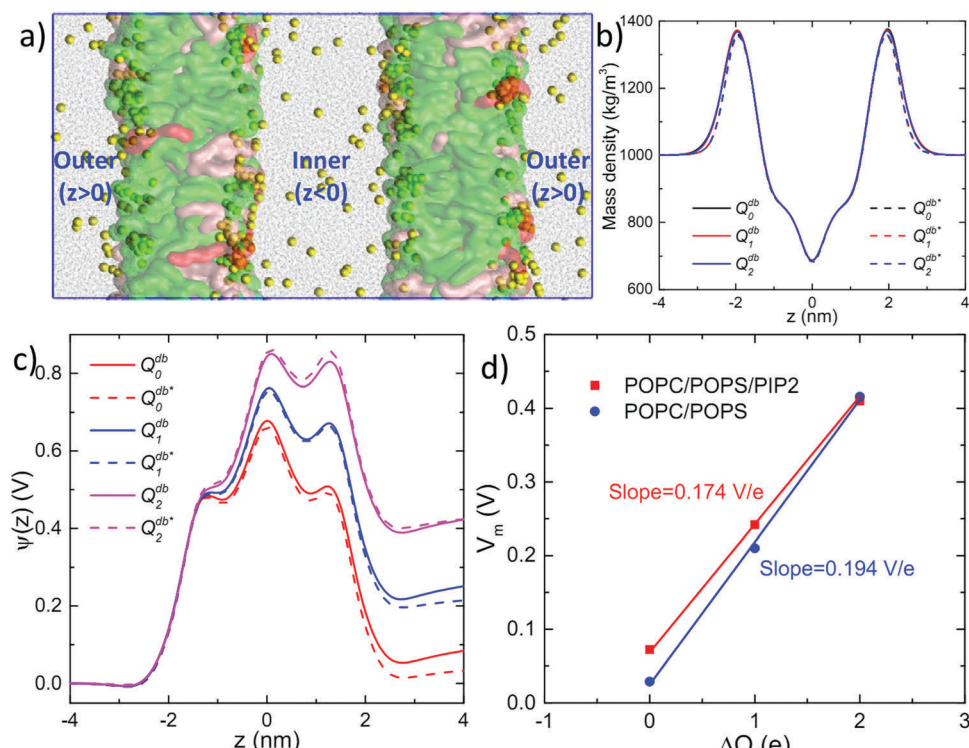


Fig. 3 PIP2 slightly affects the dependence of  $V_m$  on the magnitude of ion gradient. (a) A snapshot of a POPC/POPS/PIP2 double-bilayer system at  $t = 0$  ns with POPC in green, POPS in pink, PIP2 in red, ions in yellow and water in grey. (b and c) Mass density (b) and  $\psi(z)$  (c) profiles for systems POPC/POPS/PIP2 ( $Q^{\text{db}}$ , solid line) and POPC/POPS ( $Q^{\text{db}*}$ , dashed line) at different ion gradients ( $\Delta Q$ ). (d) Relationship of  $V_m$  to  $\Delta Q$ .

happened in the inner leaflet, reflecting the  $\psi(z)$  gradient (Fig. 1c). This phenomenon has not been observed in previous  $V_m$  modeling of a POPC bilayer.<sup>10,14</sup> The difference may be due to the use of a united atom model in the previous study or the presence of PIP2 in the current work, which has a small effect on  $V_m$  (see below). No significant effect was observed on the saturated sn-1 chain (Fig. S4, ESI†), and the structure of PIP2 could not be evaluated with confidence because of the poor statistics (the number of PIP2 in the membrane is small).

#### PIP2 slightly affects the dependence of $V_m$ on the magnitude of ion gradient

To check if 5% PIP2 content affects  $V_m$  generation, we compared POPC/POPS/PIP2 ( $Q^{db}$ ) and POPC/POPS ( $Q^{db*}$ ) double bilayer systems simulated under the *NPT* ensemble for 1  $\mu$ s (Fig. 3a).

Comparison of the  $\psi(z)$  profiles calculated separately for each bilayer of the double-bilayer and over nine 100 ns time blocks suggests a well-converged system (Fig. S5, ESI†). Subsequent comparison of  $Q^{db}$  and  $Q^{db*}$  using the last 500 ns of the data revealed that the incorporation of PIP2 slightly increases the membrane thickness (Fig. 3b) and decreases the sensitivity of  $\psi(z)$  (Fig. 3c) and  $V_m$  (Fig. 3d) to the charge gradient,  $Q$ . Similar to our  $Q^{sbv}$  and  $E^{sbv}$  systems (Fig. S3a, ESI†),  $V_m$  has only a small effect on the thickness of the membrane even when the simulations are extended to 1  $\mu$ s. Again, as in  $Q^{sbv}$  and  $E^{sbv}$ ,  $V_m$  exhibits a linear relationship with  $\Delta Q$  in systems  $Q^{db}$  and  $Q^{db*}$ . However, the slope in the latter is larger (Fig. 3d), suggesting that the presence of 5% PIP2 slightly decreased the dependence of  $V_m$  on  $\Delta Q$ . Though not the focus of this paper, the slope of the  $V_m$  vs.  $\Delta Q$  plot can be used to estimate the capacitance ( $C$ ) of each bilayer model using  $C = \Delta Q/V_m$ . Such a calculation suggests that PIP2 slightly decreases membrane

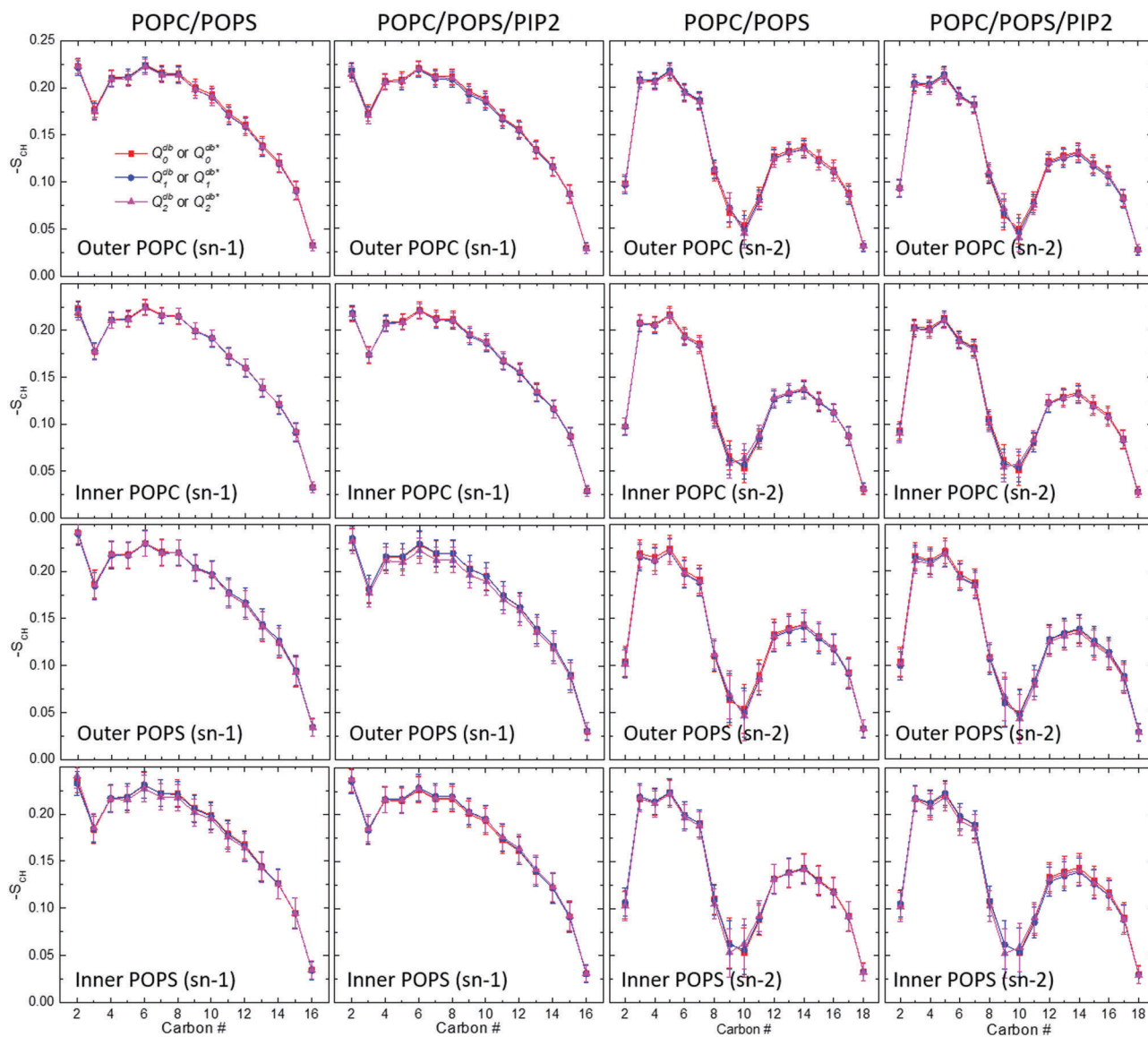


**Fig. 4** No significant difference in the lipid chain order between system  $Q^{db}$  (POPC/POPS/PIP2) and  $Q^{db*}$  (POPC/POPS). Lipid chain order parameters are shown as mean  $\pm$  SEM.  $V_m$  has no effect on lipid dynamics in systems  $Q^{db}$  and  $Q^{db*}$  likely due to its small magnitude.

capacitance. However, this effect appears to be too small to result in measurable differences between systems db and db\* in terms of lipid dynamics (Fig. 4).

### NPT simulations of single-bilayer models confirm that $V_m$ modulates the structure of lipids

In order to more effectively capture potential  $V_m$ -induced changes in membrane structure or dynamics, we used single-bilayer systems with relatively large  $E_z$ :  $E_{88}^{\text{sb}}$  and  $E_{176}^{\text{sb}}$ . These simulations resulted in larger  $V_m$  values (Fig. 5) than our simulations with a

vacuum (system  $E^{\text{sbv}}$ , Fig. 1). In both cases,  $V_m$  is linearly correlated to  $E_z$  but the slopes are different: 8.6 in  $E^{\text{sbv}}$  and 10.1 in  $E^{\text{sb}}$ . The latter is very close to the average length of the simulation box along the z-axis ( $L_z = 10.68 \text{ nm}$ ), supporting the empirical relation  $V_m = E_z \times L_z^{20,21}$  to estimate  $V_m$  in complex membranes.

To examine the overall structure of the bilayer in systems  $E_{88}^{\text{sb}}$  and  $E_{176}^{\text{sb}}$  relative to  $E_0^{\text{sb}}$ , we calculated the average area per lipid ( $A_{\text{av}}$ ). As shown in Fig. 5d,  $A_{\text{av}}$  progressively increases with increasing  $V_m$ . The change in  $A_{\text{av}}$  is more notable in these

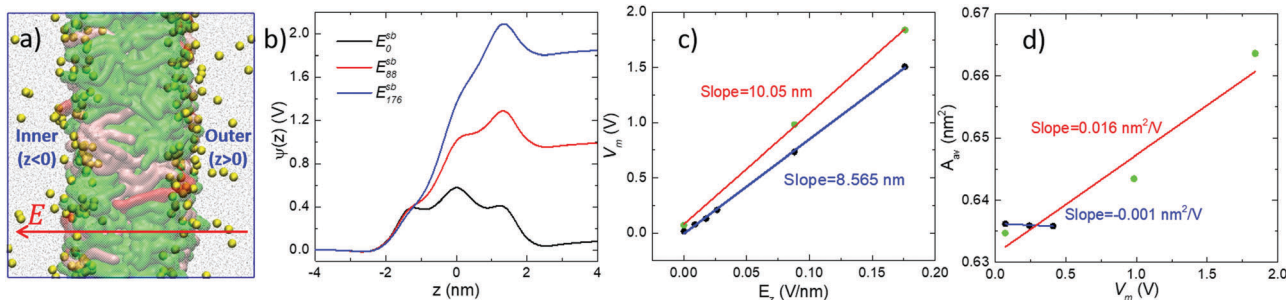


**Fig. 5**  $V_m$  modeling with system  $E^{\text{sb}}$ . (a) A snapshot at  $t = 0$  ns with POPC in green, POPS in pink, PIP2 in red, ions in yellow and water in grey. (b) Electrostatic potential profiles  $\psi(z)$  generated by different electric field strengths  $E_z$ . (c) Linear correlation between  $V_m$  and  $E_z$  for the sb (red line) and sbv (blue line) systems. (d) Average area per lipid ( $A_{\text{av}}$ ) versus  $V_m$  for sb (red line) and sbv (blue) systems.

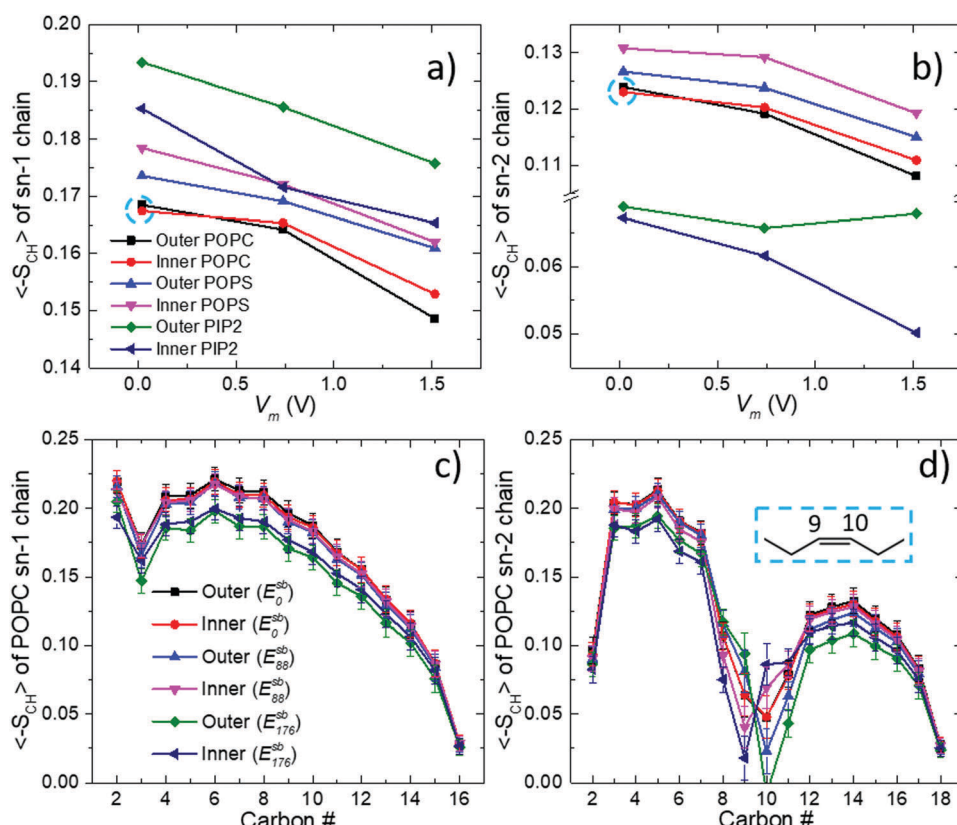


**Fig. 6**  $V_m$  promotes the dynamics of acyl chains. (a and b) Ensemble- and chain-averaged order parameters for the sn-1 (a) and sn-2 (b) tails of each lipid type at three different  $V_m$  values from systems  $E_0^{\text{sb}}$  (black and red for the outer and inner leaflets),  $E_{88}^{\text{sb}}$  (blue and magenta) and  $E_{176}^{\text{sb}}$  (green and dark blue). (c and d) Ensemble-averaged order parameter per carbon atom for the sn-1 (c) and sn-2 (d) tails of each lipid type at the same three different  $V_m$  values, where the data are shown as mean  $\pm$  SEM. Note the identical (i.e., converged) average order parameter for the POPC lipids in the outer and inner leaflets in the absence of  $V_m$  (cyan dashed circles in a and b).

simulations than in  $Q^{\text{db}}$ , suggesting that the double-bilayer system also limits lateral fluctuations, similar to the *NVT* runs in the presence of vacuum. This explains the differences in  $V_m$  generated by our single-bilayer and double-bilayer models.

For a more detailed analysis of lipid dynamics, we focused on the fluctuations of the acyl chain and head-group of the POPC lipids that dominate the system. Fig. 6a and b show the time- and chain-averaged order parameter  $\langle -S_{\text{CH}} \rangle$  for the sn-1 and sn-2 tails, indicating that  $V_m$  generally promotes disorder. To identify the region of the bilayer that is most sensitive to  $V_m$ , we show  $-S_{\text{CH}}$  per carbon atom in Fig. 6c and d. For the sn-1 tail, there is a consistent  $V_m$ -dependent decrease in  $-S_{\text{CH}}$  from the second carbon all the way to the 14th carbon, especially for  $V_m = 1839$  mV (system  $E_{176}^{\text{sb}}$ ). There is a similar trend in the sn-2 tail, where we find that the *cis* double bond between the 9th and 10th carbon atoms is especially sensitive to changes in  $V_m$  (see the inset in Fig. 6d). For the POPC lipids in the outer leaflet where the electric field was applied, carbon 9 becomes progressively more ordered and carbon 10 becomes disordered upon increasing  $V_m$ . The reverse is true for lipids in the lower leaflet.

We analyzed the POPC head-group orientation in terms of the angle  $\theta$  between a P-to-N vector and the membrane normal (Fig. 7). The results show that  $V_m$  generally increases  $\theta$  of the

outer leaflet lipids and decreases  $\theta$  of the inner leaflet lipids (Fig. 7b). This is an expected response of lipid head-group dipoles to  $V_m$ , considering the direction of the applied electric field. However,  $V_m$  has a comparatively small and similar effect on the rate of the dipole fluctuations (slightly reducing the relaxation time) on the outer and inner leaflet lipids, as suggested by the rotational autocorrelation function  $C(\tau)$  (Fig. 7c and d). These changes in the dynamics of dipoles at the head-group, though small, can have important consequences, such as on the dynamics of interfacial water molecules.<sup>14,41</sup> We note that previous MD simulation studies did not observe a major structural effect of  $V_m$  on lipid head-group dipoles,<sup>10,12,14</sup> probably due to averaging out of opposite effects on the two monolayers. Our results show that  $V_m$  values larger than the physiologic range – but not too large to cause pore formation – have a significant impact on the bilayer structure (Fig. S5, ESI†). The differential effect of  $V_m$  on the dipoles of the outer and inner monolayers could have a stronger effect on the bilayer structure if the total lateral area of the monolayers was allowed to fluctuate independently; this is not the case in our setup but possible in real membranes. One approach to allow independent dynamics of monolayers would be to run *NPT* simulations with adaptively varied total number of lipids, along the line of *N*-varied dissipative particle dynamics simulation.<sup>42–44</sup>

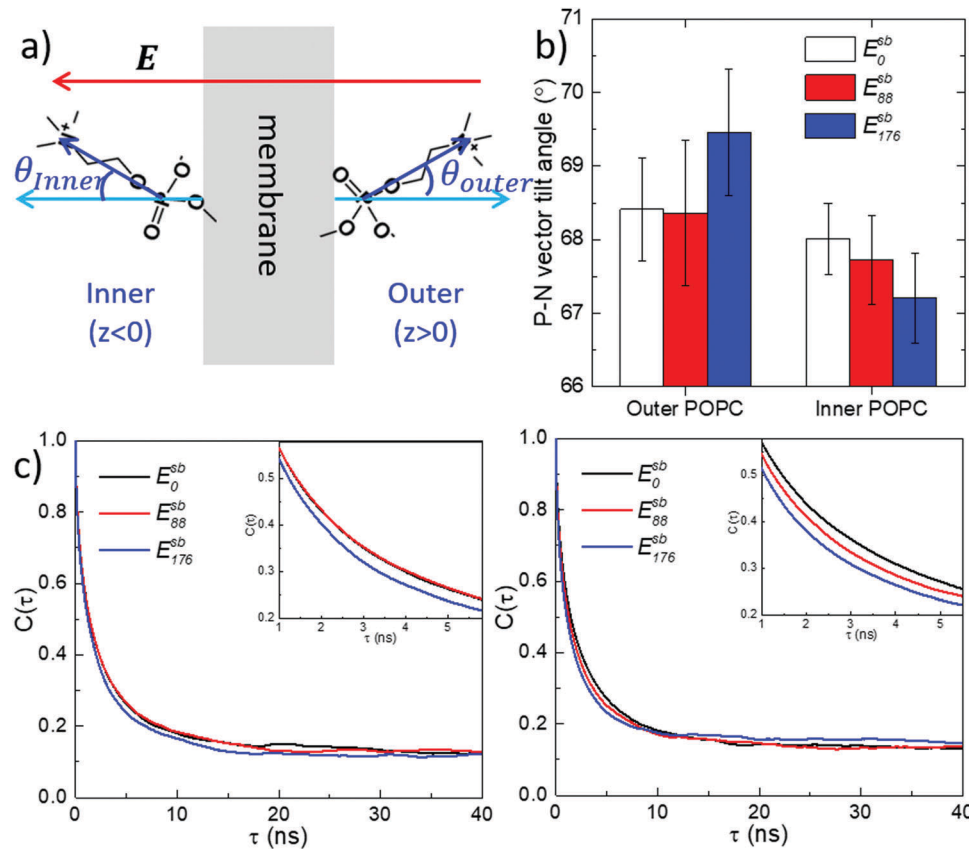


Fig. 7 Effect of  $V_m$  on the dynamics of lipid head-groups. (a) Illustration of head-group tilt angle ( $\theta$ ) defined as the angle between a P–N vector (blue arrow) and the membrane normal (light blue arrow), with the direction of the applied electric field shown by the red arrow. (b) P–N vector tilt angle averaged over POPC lipids in each leaflet from three simulations. (c) The first-rank rotational autocorrelation function ( $C(\tau)$ ) of the tilt angle for POPC lipids in the outer (left) and inner (right) leaflets. The insets show a zoom-in of the faster timescale fluctuations.

## Discussion

In this work, all-atom MD simulations were used in three different approaches to model  $V_m$ : (1) single-bilayer with vacuum using either  $\Delta Q$  ( $Q^{sbv}$ ) or  $E$  ( $E^{sbv}$ ) under *NVT*; (2) double-bilayer with  $\Delta Q$  ( $Q^{db}$ ) under *NPT*; (3) single-bilayer with  $E$  ( $E^{sb}$ ) under *NPT*. In all cases, the generated  $V_m$  was linearly correlated to the source  $\Delta Q$  or  $E_z$ . Both  $\Delta Q$  and  $E$  yielded similar electrostatic potential profiles in simulations with *NVT* or *NPT*, confirming the usefulness of  $\Delta Q$  or  $E$  to generate  $V_m$ , as reported for pure POPC bilayers.<sup>10,14</sup>  $\Delta Q$  is discrete in the single-point charge model used in this work, and has a non-zero minimum value of 2 in the *NVT* simulations (system  $Q_2^{sbv}$ ) and 1 in the *NPT* simulations (system  $Q_1^{db}$ ). Both yielded a relatively large  $V_m$  (554 mV and 240 mV). In contrast, the continuous  $E_z$  yielded  $V_m$  close to physiological values (Fig. 1 and 3). Hence, we propose that  $E$  rather than  $\Delta Q$  is more suitable for generating physiologically relevant  $V_m$  (10–100 mV) by MD simulations.

The shape of the electrostatic potential  $\psi(z)$  profiles varies among different model systems (Fig. 1, 3 and 5) and among force fields (*e.g.* coarse-grained models;<sup>45</sup> united-atom models;<sup>10</sup> modified Slurids all-atom model with virtual interaction sites;<sup>14</sup> and CHARMM Drude polarizable model<sup>46</sup>). An intriguing finding in the current work using the CHARMM36 all-atom model<sup>27–29</sup> is the significant effect of  $V_m$  on the dynamics of unsaturated lipids (especially *cis* double bonds), which may be ascribed to the charge distribution (Fig. S8, ESI†). This finding provides clues about how  $V_m$  preferentially induces electroporation in the liquid disordered phase,<sup>47</sup> and why it promotes membrane phase separation.<sup>48</sup> Our findings may thus inspire experimental measurements of the deuterium order parameter  $S_{CD}$  with NMR or ESR<sup>36,37</sup> in the presence of  $V_m$ . If systematically validated and proven to be universally true, the dynamics of *cis* double bonds may be a useful proxy to measure  $V_m$  in complex systems. On the MD front, whether polarization of *cis* double bonds may increase the effects of  $V_m$  is an interesting topic that requires a polarizable force field to test.

One issue raised by the current as well as previous simulations<sup>10</sup> is the nonzero  $V_m$  (typically several to tens of millivolts) in systems with no net  $\Delta Q$  or  $E_z$  (Table 1), where  $V_m$  should be zero since the bilayer is symmetric. This could be explained by differential lipid clustering in the outer and inner leaflets, which requires longer simulations to average out.<sup>49–51</sup> However, extending simulation  $Q_0^0$  to 1  $\mu$ s did not improve the results significantly (Fig. S5c and d), and the deviation from zero is always positive. These observations, along with the fact that the initial lipid distribution was similar among the various systems, suggest that the nonzero  $V_m$  is a systematic error likely caused by the local asymmetry in the ion distribution whose concentration was large in our systems. This, however, will have little effect on the trends observed in our comparative analyses of  $V_m$ , or on its impact on lipid dynamics.

## Conclusion

We have investigated the potential effects of transmembrane potential ( $V_m$ ) on the structure and dynamics of a complex

bilayer made up of POPC, POPS and PIP2 lipids. We used three different MD simulation approaches: single-bilayer models with a vacuum under the *NVT* ensemble ( $Q^{sbv}$  and  $E^{sbv}$ ), a double-bilayer model with ion imbalance ( $Q^{db}$ ) and a single-bilayer with constant electric field ( $E^{sb}$ ) under the *NPT* ensemble. Our results indicated that both the  $Q$  and  $E$  approaches generate qualitatively similar  $V_m$ s for the model membranes tested. We further found that  $V_m$  decreases the lipid acyl chain order, particularly at the *cis* double bond of the sn-2 tail. Moreover, using *NPT* simulations with system  $E^{sb}$ , we observed  $V_m$ -induced fluctuations of lipid head-groups with opposite effects on the orientation of dipoles in the two monolayers. Generally, the adjustable electric field approach enables modeling of more physiologically relevant  $V_m$ , suggesting that it is a better means of studying  $V_m$  by MD simulations.

## Conflicts of interest

The authors declare no competing financial interest.

## Acknowledgements

This work was supported in part by the National Institutes of Health Grants (R01GM100078) and by the 111 Project (B13003). We thank the Extreme Science and Engineering Discovery Environment (XSEDE, project: TG-MCB150054) and the Texas Advanced Computing Center (TACC) for generous computational resources.

## References

- 1 M. Yang and W. J. Brackenbury, Membrane Potential and Cancer Progression, *Front. Physiol.*, 2013, **4**, 185.
- 2 J. D. Ly, D. Grubb and A. Lawen, The Mitochondrial Membrane Potential ( $\Delta\psi M$ ) in Apoptosis; an Update, *Apoptosis*, 2003, **8**, 115–128.
- 3 L. B. Rosen, D. D. Ginty, M. J. Weber and M. E. Greenberg, Membrane Depolarization and Calcium Influx Stimulate Mek and Map Kinase Via Activation of Ras, *Neuron*, 1994, **12**, 1207–1221.
- 4 Y. Zhou, *et al.*, Membrane Potential Modulates Plasma Membrane Phospholipid Dynamics and K-Ras Signaling, *Science*, 2015, **349**, 873–876.
- 5 S. Chatterjee, E. A. Browning, N. Hong, K. DeBolt, E. M. Sorokina, W. Liu, M. J. Birnbaum and A. B. Fisher, Membrane Depolarization Is the Trigger for Pi3k/Akt Activation and Leads to the Generation of ROS, *Am. J. Physiol. Heart Circ. Physiol.*, 2012, **302**, H105–H114.
- 6 B. Sakmann and E. Neher, Patch Clamp Techniques for Studying Ionic Channels in Excitable Membranes, *Annu. Rev. Physiol.*, 1984, **46**, 455–472.
- 7 C. R. Cadwell, A. Palasantza, X. Jiang, P. Berens, Q. Deng, M. Yilmaz, J. Reimer, S. Shen, M. Bethge and K. F. Tolias, Electrophysiological, Transcriptomic and Morphologic Profiling of Single Neurons Using Patch-Seq, *Nat. Biotechnol.*, 2016, **34**, 199.
- 8 B. E. Steinberg, N. Touret, M. Vargas-Caballero and S. Grinstein, In Situ Measurement of the Electrical Potential across the

- Phagosomal Membrane Using Fret and Its Contribution to the Proton-Motive Force, *Proc. Natl. Acad. Sci. U. S. A.*, 2007, **104**, 9523–9528.
- 9 M. Koivusalo, B. E. Steinberg, D. Mason and S. Grinstein, In Situ Measurement of the Electrical Potential across the Lysosomal Membrane Using Fret, *Traffic*, 2011, **12**, 972–982.
- 10 L. Delemotte, F. Dehez, W. Treptow and M. Tarek, Modeling Membranes under a Transmembrane Potential, *J. Phys. Chem. B*, 2008, **112**, 5547–5550.
- 11 R. A. Böckmann, A. Hac, T. Heimburg and H. Grubmüller, Effect of Sodium Chloride on a Lipid Bilayer, *Biophys. J.*, 2003, **85**, 1647–1655.
- 12 S.-J. Lee, Y. Song and N. A. Baker, Molecular Dynamics Simulations of Asymmetric NaCl and KCl Solutions Separated by Phosphatidylcholine Bilayers: Potential Drops and Structural Changes Induced by Strong  $\text{Na}^+$ -Lipid Interactions and Finite Size Effects, *Biophys. J.*, 2008, **94**, 3565–3576.
- 13 J. N. Sachs, P. S. Crozier and T. B. Woolf, Atomistic Simulations of Biologically Realistic Transmembrane Potential Gradients, *J. Chem. Phys.*, 2004, **121**, 10847–10851.
- 14 J. Melcr, D. Bonhenry, S. T. P. N. Timr and P. Jungwirth, Transmembrane Potential Modeling: Comparison between Methods of Constant Electric Field and Ion Imbalance, *J. Chem. Theory Comput.*, 2016, **12**, 2418–2425.
- 15 X. Lin, J. H. Lorent, A. D. Skinkle, K. R. Levental, M. N. Waxham, A. A. Gorfe and I. Levental, Domain Stability in Biomimetic Membranes Driven by Lipid Polyunsaturation, *J. Phys. Chem. B*, 2016, **120**, 11930–11941.
- 16 L. Delemotte and M. Tarek, Molecular Dynamics Simulations of Lipid Membrane Electroporation, *J. Membr. Biol.*, 2012, **245**, 531–543.
- 17 A. Polak, D. Bonhenry, F. Dehez, P. Kramar, D. Miklavčič and M. Tarek, On the Electroporation Thresholds of Lipid Bilayers: Molecular Dynamics Simulation Investigations, *J. Membr. Biol.*, 2013, **246**, 843–850.
- 18 M. Tarek, Membrane Electroporation: A Molecular Dynamics Simulation, *Biophys. J.*, 2005, **88**, 4045–4053.
- 19 P. T. Vernier and M. J. Ziegler, Nanosecond Field Alignment of Head Group and Water Dipoles in Electroporating Phospholipid Bilayers, *J. Phys. Chem. B*, 2007, **111**, 12993–12996.
- 20 B. Roux, The Membrane Potential and Its Representation by a Constant Electric Field in Computer Simulations, *Biophys. J.*, 2008, **95**, 4205–4216.
- 21 J. Gumbart, F. Khalili-Araghi, M. Sotomayor and B. Roux, Constant Electric Field Simulations of the Membrane Potential Illustrated with Simple Systems, *Biochim. Biophys. Acta, Biomembr.*, 2012, **1818**, 294–302.
- 22 G. Van Meer, D. R. Voelker and G. W. Feigenson, Membrane Lipids: Where They Are and How They Behave, *Nat. Rev. Mol. Cell Biol.*, 2008, **9**, 112.
- 23 G. Di Paolo and P. De Camilli, Phosphoinositides in Cell Regulation and Membrane Dynamics, *Nature*, 2006, **443**, 651–657.
- 24 S. Jo, T. Kim, V. G. Iyer and W. Im, Charmm-Gui: A Web-Based Graphical User Interface for Charmm, *J. Comput. Chem.*, 2008, **29**, 1859–1865.
- 25 E. L. Wu, X. Cheng, S. Jo, H. Rui, K. C. Song, E. M. Dávila-Contreras, Y. Qi, J. Lee, V. Monje-Galvan and R. M. Venable, Charmm-Gui Membrane Builder toward Realistic Biological Membrane Simulations, *J. Comput. Chem.*, 2014, **35**, 1997–2004.
- 26 M. J. Abraham, T. Murtola, R. Schulz, S. Pál, J. C. Smith, B. Hess and E. Lindahl, Gromacs: High Performance Molecular Simulations through Multi-Level Parallelism from Laptops to Supercomputers, *SoftwareX*, 2015, **1**, 19–25.
- 27 J. B. Klauda, R. M. Venable, J. A. Freites, J. W. O'Connor, D. J. Tobias, C. Mondragon-Ramirez, I. Vorobyov, A. D. MacKerell Jr and R. W. Pastor, Update of the Charmm All-Atom Additive Force Field for Lipids: Validation on Six Lipid Types, *J. Phys. Chem. B*, 2010, **114**, 7830–7843.
- 28 R. M. Venable, Y. Luo, K. Gawrisch, B. Roux and R. W. Pastor, Simulations of Anionic Lipid Membranes: Development of Interaction-Specific Ion Parameters and Validation Using Nmr Data, *J. Phys. Chem. B*, 2013, **117**, 10183–10192.
- 29 W. L. Jorgensen, J. Chandrasekhar, J. D. Madura, R. W. Impey and M. L. Klein, Comparison of Simple Potential Functions for Simulating Liquid Water, *J. Chem. Phys.*, 1983, **79**, 926–935.
- 30 U. Essmann, L. Perera, M. L. Berkowitz, T. Darden, H. Lee and L. G. Pedersen, A Smooth Particle Mesh Ewald Method, *J. Chem. Phys.*, 1995, **103**, 8577–8593.
- 31 S. Nosé, A Molecular Dynamics Method for Simulations in the Canonical Ensemble, *Mol. Phys.*, 1984, **52**, 255–268.
- 32 W. G. Hoover, Canonical Dynamics: Equilibrium Phase-Space Distributions, *Phys. Rev. A: At., Mol., Opt. Phys.*, 1985, **31**, 1695.
- 33 M. Parrinello and A. Rahman, Polymorphic Transitions in Single Crystals: A New Molecular Dynamics Method, *J. Appl. Phys.*, 1981, **52**, 7182–7190.
- 34 B. Hess, H. Bekker, H. J. Berendsen and J. G. Fraaije, Lincs: A Linear Constraint Solver for Molecular Simulations, *J. Comput. Chem.*, 1997, **18**, 1463–1472.
- 35 W. Humphrey, A. Dalke and K. Schulten, Vmd: Visual Molecular Dynamics, *J. Mol. Graphics*, 1996, **14**, 33–38.
- 36 J. H. Davis, The Description of Membrane Lipid Conformation, Order and Dynamics by 2h-Nmr, *Biochim. Biophys. Acta*, 1983, **737**, 117–171.
- 37 M. R. de Planque, D. V. Greathouse, R. E. Koeppe, H. Schäfer, D. Marsh and J. A. Killian, Influence of Lipid/Peptide Hydrophobic Mismatch on the Thickness of Diacylphosphatidylcholine Bilayers. A 2h Nmr and Esr Study Using Designed Transmembrane A-Helical Peptides and Gramicidin A, *Biochemistry*, 1998, **37**, 9333–9345.
- 38 Y. Cote, P. Senet, P. Delarue, G. G. Maisuradze and H. A. Scheraga, Nonexponential Decay of Internal Rotational Correlation Functions of Native Proteins and Self-Similar Structural Fluctuations, *Proc. Natl. Acad. Sci. U. S. A.*, 2010, **107**, 19844–19849.
- 39 P. Prakash, Y. Zhou, H. Liang, J. F. Hancock and A. A. Gorfe, Oncogenic K-Ras Binds to an Anionic Membrane in Two Distinct Orientations: A Molecular Dynamics Analysis, *Biophys. J.*, 2016, **110**, 1125–1138.

- 40 Z.-L. Li and M. Buck, Computational Modeling Reveals That Signaling Lipids Modulate the Orientation of K-Ras4a at the Membrane Reflecting Protein Topology, *Structure*, 2017, **25**(679–689), e2.
- 41 L. Janosi and A. A. Gorfe, Simulating Popc and Popc/Popg Bilayers: Conserved Packing and Altered Surface Reactivity, *J. Chem. Theory Comput.*, 2010, **6**, 3267–3273.
- 42 B. Hong, F. Qiu, H. Zhang and Y. Yang, Budding Dynamics of Individual Domains in Multicomponent Membranes Simulated by N-Varied Dissipative Particle Dynamics, *J. Phys. Chem. B*, 2007, **111**, 5837–5849.
- 43 T. Yue and X. Zhang, Molecular Understanding of Receptor-Mediated Membrane Responses to Ligand-Coated Nanoparticles, *Soft Matter*, 2011, **7**, 9104–9112.
- 44 T. Yue, S. Li, X. Zhang and W. Wang, The Relationship between Membrane Curvature Generation and Clustering of Anchored Proteins: A Computer Simulation Study, *Soft Matter*, 2010, **6**, 6109–6118.
- 45 D. S. Bruhn, M. A. Lomholt and H. Khandelia, Quantifying the Relationship between Curvature and Electric Potential in Lipid Bilayers, *J. Phys. Chem. B*, 2016, **120**, 4812–4817.
- 46 H. Li, J. Chowdhary, L. Huang, X. He, A. D. MacKerell and B. Roux, Drude Polarizable Force Field for Molecular Dynamics Simulations of Saturated and Unsaturated Zwitterionic Lipids, *J. Chem. Theory Comput.*, 2017, **13**, 4535–4552.
- 47 J. T. Sengel and M. I. Wallace, Imaging the Dynamics of Individual Electropores, *Proc. Natl. Acad. Sci. U. S. A.*, 2016, **113**, 5281–5286.
- 48 J. Malinsky, W. Tanner and M. Opekarova, Transmembrane Voltage: Potential to Induce Lateral Microdomains, *Biochim. Biophys. Acta, Mol. Cell Biol. Lipids*, 2016, **1861**, 806–811.
- 49 L. Janosi, Z. Li, J. F. Hancock and A. A. Gorfe, Organization, Dynamics, and Segregation of Ras Nanoclusters in Membrane Domains, *Proc. Natl. Acad. Sci. U. S. A.*, 2012, **109**, 8097–8102.
- 50 Z. Li, L. Janosi and A. A. Gorfe, Formation and Domain Partitioning of H-Ras Peptide Nanoclusters: Effects of Peptide Concentration and Lipid Composition, *J. Am. Chem. Soc.*, 2012, **134**, 17278–17285.
- 51 X. Lin, Z. Li and A. A. Gorfe, Reversible Effects of Peptide Concentration and Lipid Composition on H-Ras Lipid Anchor Clustering, *Biophys. J.*, 2015, **109**, 2467–2470.